THE ASTROPHYSICAL JOURNAL, 472:611–623, 1996 December 1

STAR FORMATION ACTIVITY IN THE LARGE MAGELLANIC CLOUD: FAR-INFRARED EMISSION FROM *IRAS* HIGH-RESOLUTION DATA

DOUGLAS A. CALDWELL[1] AND MARC L. KUTNER
National Radio Astronomy Observatory,[2] 949 North Cherry Avenue, Campus Building 65, Tucson, AZ 85721-0655
Received 1995 July 25; accepted 1996 June 25

ABSTRACT

We present an investigation of the properties of 21 molecular clouds in the LMC. Our data consist of 60 μm and 100 μm *IRAS* images that we compare with fully sampled ^{12}CO ($J = 1 \rightarrow 0$) maps. The CO data were taken on the 15 m Swedish-ESO Submillimeter Telescope (SEST), which has a beamwidth at 2.6 mm of 45″, or 10 pc at the distance of the LMC. We use the *IRAS* high-resolution reprocessed data, with approximate resolutions of 60″ and 75″ at 60 μm and 100 μm, respectively. The clouds mapped are in three regions: two complexes south of 30 Doradus, and one at the H II region N11. We measure the far-infrared luminosities for each cloud that has a good CO-FIR correspondence and compare these results with those from similar studies done on Milky Way molecular clouds. The far-infrared luminosities range from 3.5×10^4 to 2.8×10^6 $L_\odot$, with an average value of 4×10^5 $L_\odot$. This average is lower than that seen for H II regions in the inner Milky Way, as reported by Scoville & Good in 1989 and slightly higher than that for outer Galaxy clouds as reported by Mead et al. in 1990. Virial masses of these clouds are from 4×10^4 to 1×10^6 $M_\odot$. Star formation activity ($L_{\rm FIR}/M_{\rm VIR}$), defined as the ratio of the luminosity from recently formed stars to the total cloud mass, has a range of 2 orders of magnitude for any $M_{\rm VIR}$. In addition, we find that $L_{\rm FIR}/M_{\rm VIR}$ is independent of cloud mass over the entire range of measured virial masses. These results indicate that although less luminous in CO and FIR than their inner Milky Way counterparts, LMC molecular clouds are undergoing significant massive star formation. $L_{\rm FIR}$ is used to determine the numbers and types of stars embedded in the GMCs. We compare these findings with those from the Milky Way and discuss the implications for star formation theories.

Subject headings: galaxies: ISM — infrared: galaxies — ISM: clouds — ISM: molecules — Magellanic Clouds — stars: formation

1. INTRODUCTION

Though it is accepted that molecular clouds are the birthplaces of stars, the details of cloud evolution and star formation are poorly understood. There are two large-scale scenarios for cloud evolution that have been actively pursued. In one picture, larger clouds are built out of smaller clouds (see, e.g., Scalo 1985 and references therein). Massive star formation takes place when some mass threshold is reached, so that gravity can overcome the magnetic and turbulent support of the cloud. The alternative scenario has the largest structures forming first (see, e.g., Elmegreen 1993 and references therein). The largest structures have masses of about 10^7 $M_\odot$, and they are generally H I. Within these structures are the GMC complexes and individual clouds. Star formation can take place in any of the structures when the local conditions are right.

In order to understand star formation on a galactic scale, we must first determine which of these general pictures holds for the formation of molecular clouds. We then decide which local conditions are important in determining star formation efficiency and the initial mass function. In order to do this, we must study molecular clouds and star formation under different conditions. The easiest way to provide different conditions is to look in different galactic environments.

One environment that is being studied extensively is the outer Galaxy. Detailed CO maps of some three dozen clouds are reported in Mead (1988) and Mead & Kutner (1988). Mead et al. (1987) used the Kuiper Airborne Observatory to detect far-infrared (FIR) emission from four outer Galaxy clouds, suggesting that these clouds are forming O and B stars. Mead, Kutner, & Evans (1990) showed that FIR luminosity, $L_{\rm FIR}$, can be used as a measure of massive star formation. They made 6 cm VLA observations of molecular clouds in the outer Galaxy for which they had *IRAS* FIR data. A comparison of the rate of ionizing photon production, N_L, from thermal radio sources associated with molecular clouds and $L_{\rm FIR}$ for the clouds showed that their sources were consistent with a single zero-age main-sequence star or a cluster of stars. In either case, the ionizing photons measure the most luminous star present because of the rapid increase of N_L with stellar luminosity. They conclude that because of the good fit of both the radio and FIR data with theory, both are good tracers of massive star formation.

The important results of these outer Galaxy studies relevant to this work, which have been confirmed by other groups (see, e.g., Wouterloot, Henkel, & Walmsley 1989), can be summarized as follows:

1. Most of the emission appears to be coming from clouds with GMC-type dimensions (i.e., tens of pc in extent), though the masses of the largest clouds ($\sim 2 \times 10^5$ $M_\odot$) are smaller than those of the largest inner Galaxy GMCs.
2. The cloud envelopes appear a factor of $\sim$2 less luminous in CO per unit virial mass than their inner Galaxy counterparts.

[1] Current address: Department of Physics, Applied Physics and Astronomy, Rensselaer Polytechnic Institute, Troy, NY 12180.

[2] The National Radio Astronomy Observatory is operated by Associated Universities, Inc., under a cooperative agreement with the National Science Foundation.

3. The star formation activity, defined as the ratio of the luminosity of stars currently forming to the total cloud mass, has the same wide range of values as seen in the inner Galaxy (i.e. molecular ring).

The Magellanic Clouds provide unique opportunities to study molecular clouds and star formation in galaxies whose interstellar environment is very different from that in the Milky Way. The Magellanic Clouds are very metal poor compared with the Milky Way. The Large Magellanic Cloud (LMC) has C and O abundances of 0.27 and 0.5 times the Milky Way values, respectively (Dufour 1984). In addition, the interstellar radiation field in the LMC is stronger than in the Milky Way (Israel et al. 1986), and the dust-to-gas ratio, $E(B-V)/N_{\rm H}$, is 0.25 times that of the Milky Way (Koornneef 1984; Bouchet et al. 1985).

The 15 m Swedish-ESO Submillimeter Telescope (SEST) allows for mapping of CO emission from individual GMCs in the Magellanic Clouds. With an angular resolution of 45″ at 2.6 mm, the SEST provides a linear resolution on the LMC of 10 pc in the CO ($J = 1 \rightarrow 0$) line. This is well suited to measure the properties of clouds that are a few tens of pc in extent.

The study of CO emission from the Magellanic Clouds has been carried out as a Key Programme for the SEST. The goal of the program was to produce fully sampled maps of a large number of individual molecular clouds. The resolution and sensitivity of these observations allows virial masses to be determined for a statistically significant sample of clouds. In addition to measuring cloud masses, we can also compare, on a cloud-by-cloud basis, star formation and star-forming regions in the Magellanic Clouds and the Milky Way.

In order to study star formation in the Magellanic Clouds, we have used *IRAS* High Resolution (HIRES) data. In this paper, we present the results of these HIRES studies of the LMC. Comparing the SEST and *IRAS* data, we found 21 clouds in three regions of the LMC with good CO-FIR correspondence. We use the FIR data as a measure of the amount of massive star formation in the GMC. The ratio $L_{\rm FIR}/M_{\rm VIR}$ is used as a measure of the star formation activity of the cloud. This ratio gives an indication of the amount of star formation per unit cloud mass. It allows us to compare clouds over a large range of masses to determine how actively they are forming stars.

This work is part of a larger effort to study star formation in different environments, including the Small Magellanic Cloud, the outer Milky Way, and M31. The SMC results will be presented in Caldwell & Kutner (1997), and a detailed analysis of the statistical properties of GMCs in these environments is under way.

2. OBSERVATIONS AND DATA REDUCTION

We have mapped three regions in the LMC, covering a wide range in both FIR and CO emission and morphology. They are 30DOR-CENTER, centered at (J2000) R.A. = $5^{\rm h}39^{\rm m}28^{\rm s}$, decl. = $-70°18'31''$; 30DOR-SOUTH, at R.A. = $5^{\rm h}39^{\rm m}19^{\rm s}$, decl. = $-71°08'31''$; and N11 at R.A. = $4^{\rm h}57^{\rm m}06^{\rm s}$, decl. = $-66°24'28''$. The CO data are in the form of fully sampled ^{12}CO ($J = 1 \rightarrow 0$) maps of selected GMCs. The SEST project is discussed in Israel et al. (1993). The LMC CO data for the 30 Dor region are analyzed in detail in Kutner et al. (1996a, 1996b). The N11 data are analyzed in detail by de Graauw et al. (1996).

The *IRAS* HIRES data are the original *IRAS* survey scans reprocessed using the Maximum Correlation Method (MCM) algorithm of Aumann, Fowler, & Melnyk (1990). The MCM algorithm relies on oversampling in the *IRAS* survey; thus, the resolution will depend on the coverage of the given region. The resolution can also vary somewhat over a given image. A description of the *IRAS* instrument array and the survey can be found in the *IRAS* Explanatory Supplement. A complete description of the data products, processing, and baselining unique to the HIRES data set can be found in the Infrared Processing and Analysis Center (IPAC) User's Guide (IPAC User's Guide 1993) and the Laundr and Yoric Software Design Specifications (Fowler & Melnyk 1990a, 1990b).

We used three 1 deg^2 image fields in the LMC, fields centered on 30DOR-CENTER, 30DOR-SOUTH, and N11. The images all have 15″ × 15″ pixels. The default HIRES baselining was used for all three regions. This involves removing a linear baseline from each survey scan in the image, with no cross-scan flat-fielding. The MCM algorithm is an iterative process. The data products are output at different iteration numbers to monitor the convergence. Our data are from the default outputs: one, five, 10, and 20 iterations. For all of our fields, the 20th iteration data of the source regions show the best resolution and the smallest correction factor variance. The resulting resolution of the FIR maps is approximately 60″ at 60 μm and 75″ at 100 μm. There is little variation (less than 7% maximum) in the resolution across the regions of significant emission.

It is important to determine if the algorithm has sufficiently converged or if additional processing would yield significant improvement to the image. With the HIRES data, there are several means to check for convergence. Low values of the correction factor variance in the regions of strong source emission indicate that the fluxes of those pixels are well agreed upon by each detector footprint that covers that pixel. For each of our three images, the correction factor variance was low (≤ 0.2) in the regions of interest. This is not proof of image convergence, though, because the correction factor variance will go to zero if the iteration is continued long enough. As another check for algorithm convergence, χ^2 values for the calculated image footprint fluxes are given at each iteration. The values are an indication of how close the calculated image, when viewed with the original *IRAS* detector coverage, is to the actual *IRAS* data. This can be used to see if the HIRES image is a good approximation of the actual region under observation. The noise-weighted χ^2/N after the 20th iteration for the footprints with flux $> 5\%$ of the peak image flux (see Aumann et al. 1990) are 0.62, 1.79, and 1.81 at 60 μm for the N11, 30DOR-SOUTH, and 30DOR-CENTER regions, respectively. The χ^2/N values at 100 μm for N11, 30DOR-SOUTH, and 30DOR-CENTER are 1.31, 0.76, and 2.04, respectively. These values indicate a reasonable fit of the calculated image fluxes to the *IRAS* data and, along with the low correction factor variance values, indicate sufficient convergence of the reprocessing algorithm.

The uniform detector coverage of our source regions indicates that the observed structure is due to more than just coverage variations. In addition, the low values of the correction factor variance maps in the regions of significant emission indicate that peaks are not a result of noisy footprints or other processing artifacts, which would give a high variance in the affected pixels.

One final check of our HIRES data is comparison with a far-infrared map made with the Kuiper Airborne Observatory (KAO) 0.9 m telescope using D. A. Harper's Photometer Camera. We had one flight in 1991 March and were able to map the N159 region south of 30 Doradus at 160 μm with a resolution of $\sim$45″. This map shows a good correspondence between the KAO and HIRES measured emission at 100 μm. These results are presented in Caldwell & Kutner (1993).

The FIR images were processed using the AIPS image processing system. The HIRES data include baselining in the processing; therefore, the background levels of our images are generally small. In order to remove the remaining background not associated with individual molecular clouds, a plane was fitted to pixels surrounding the emission. The value of the background plane at each cloud was subtracted from the intensity measure of the cloud. For most clouds, the background level was only $\sim$0.1–0.2 times the peak intensity.

3. RESULTS

We have compared CO and FIR emission in three regions of the LMC: 30DOR-CENTER, 30DOR-SOUTH, and N11, as shown in Figures 1, 2, and 3, respectively. These figures contain both the 60 μm and 100 μm emission on top of the CO ($J = 1 \rightarrow 0$) integrated intensity.

In these regions, we have identified 21 individual molecular clouds for which there is a good CO-FIR correspondence. The cloud names and locations are given in Table 1. The source name appears in column (1). Column (2) lists the SEST Key Programme names of the CO peak(s) associated with each source. The third column contains the Leiden

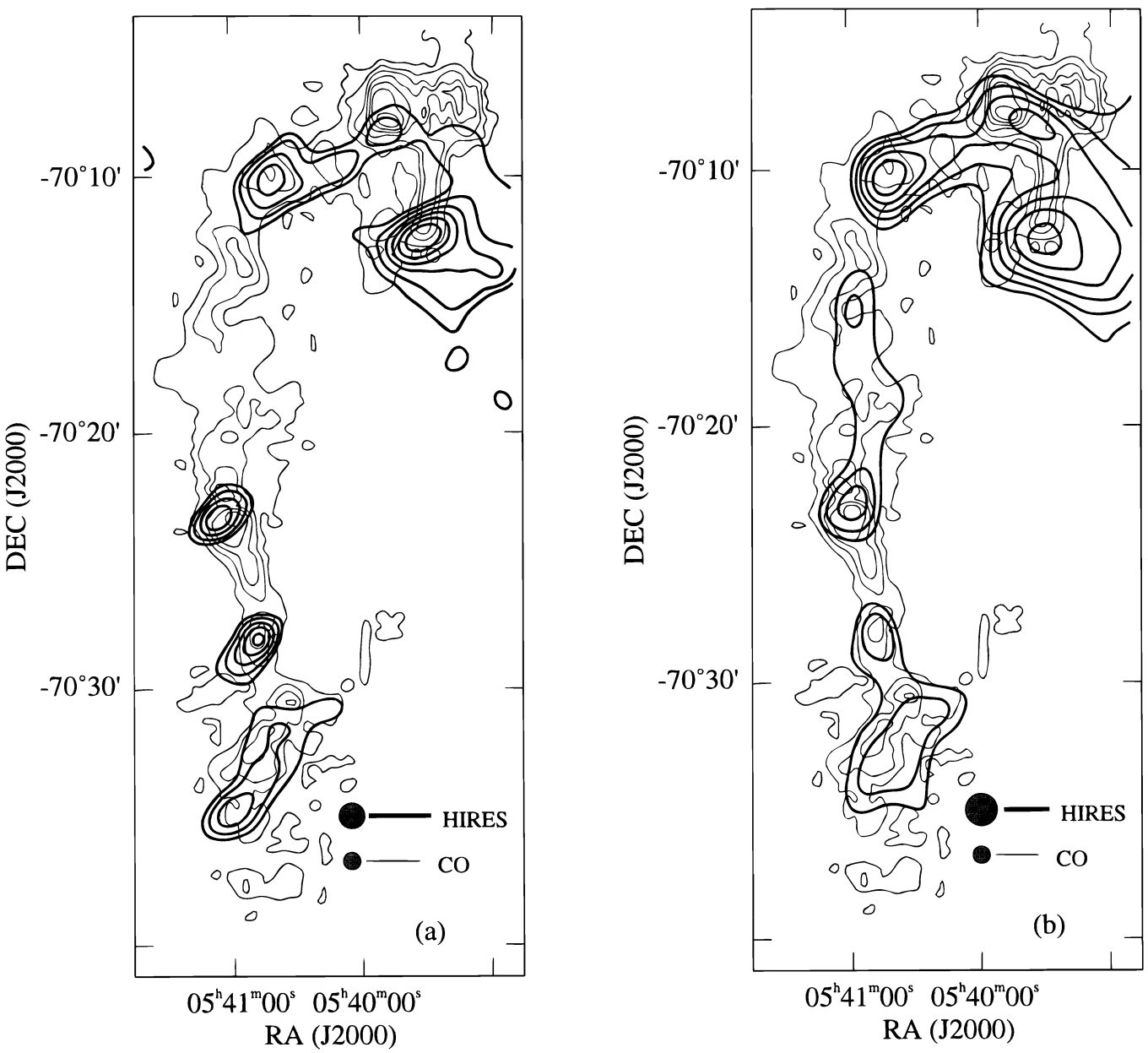

FIG. 1.—30DOR-CENTER *IRAS* HIRES emission maps shown with CO ($J = 1 \rightarrow 0$) integrated intensity (*light contours*) for comparison. (*a*) 60 μm map with log spaced contours at 10, 14, 21, 30, 43, 62, 90 MJy sr^{-1}. (*b*) 100 μm map with log spaced contours at 30, 38, 48, 60, 75, 95 MJy sr^{-1}. The CO ($J = 1 \rightarrow 0$) contours are 1, 4, 8, 12, 16, 20, 24, 28, 32 K km s^{-1} in both figures. Note: the CO data do not extend over the full area of the map; therefore, some of the lowest contours are not closed.

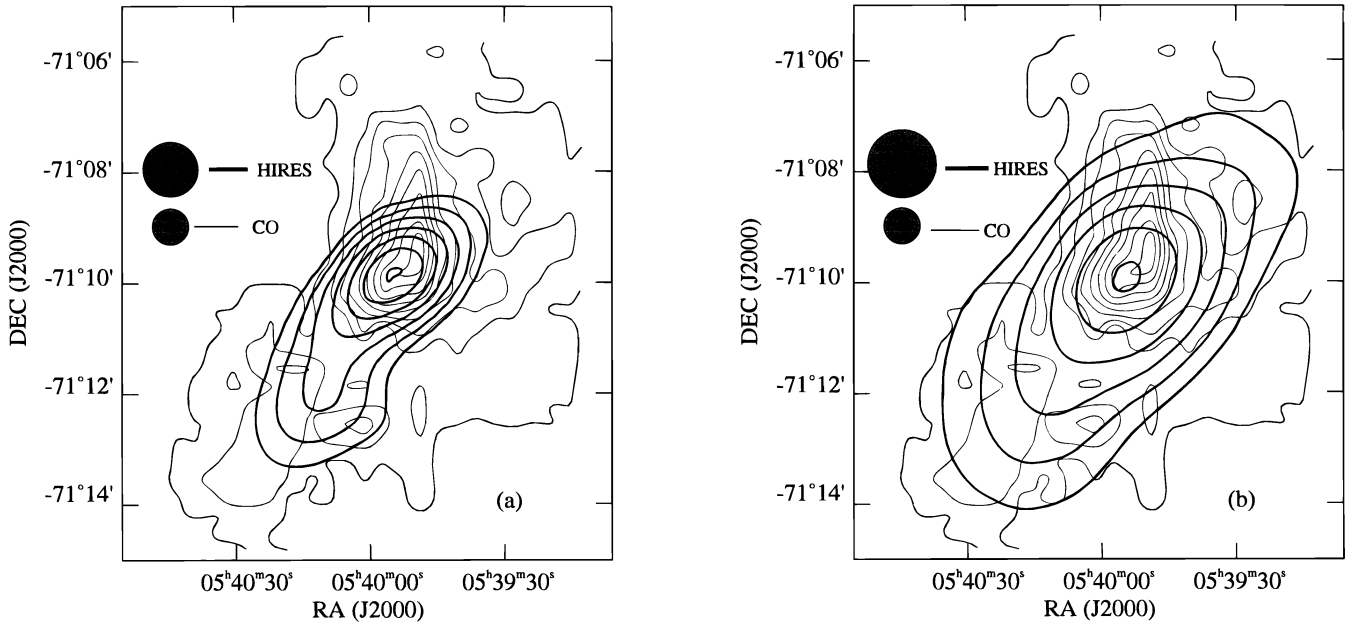

FIG. 2.—30DOR-SOUTH *IRAS* HIRES emission maps shown with CO ($J = 1 \rightarrow 0$) integrated intensity (*light contours*) for comparison. (*a*) 60 μm map with log spaced contours at 10, 19, 37, 72, 139, 269, 520 MJy sr^{-1}. (*b*) 100 μm map with log spaced contours at 15, 28, 51, 94, 174, 320 MJy sr^{-1}. The CO ($J = 1 \rightarrow 0$) contours are 1, 3, 5, 7, 9, 11, 13, 15 K km s^{-1} in both figures. Note: the CO data do not extend over the full area of the map; therefore, some of the lowest contours are not closed.

IRAS-LMC (LI-LMC) catalog number (Schwering 1989) for sources that match the positions of our clouds. The fourth and fifth columns contain the equatorial coordinates of the 60 μm peak of each cloud. The results of the FIR measurements are presented in Table 2. The source names are listed in column (1). Column (2) contains the area of the cloud used in calculating the total far-infrared luminosity. Columns (3) and (4) list the 60 μm and 100 μm mean intensities for each of the clouds observed. The 60 μm and 100 μm intensities are the averages over the pixels at which the emission is above the local background for the clouds where emission boundaries are evident. The sizes of the clouds are determined from the extent of the FIR emission where possible. In the cases with no obvious FIR boundary, the extent of the CO emission is used. The cloud areas given here are the numbers of HIRES pixels at which the 60 μm

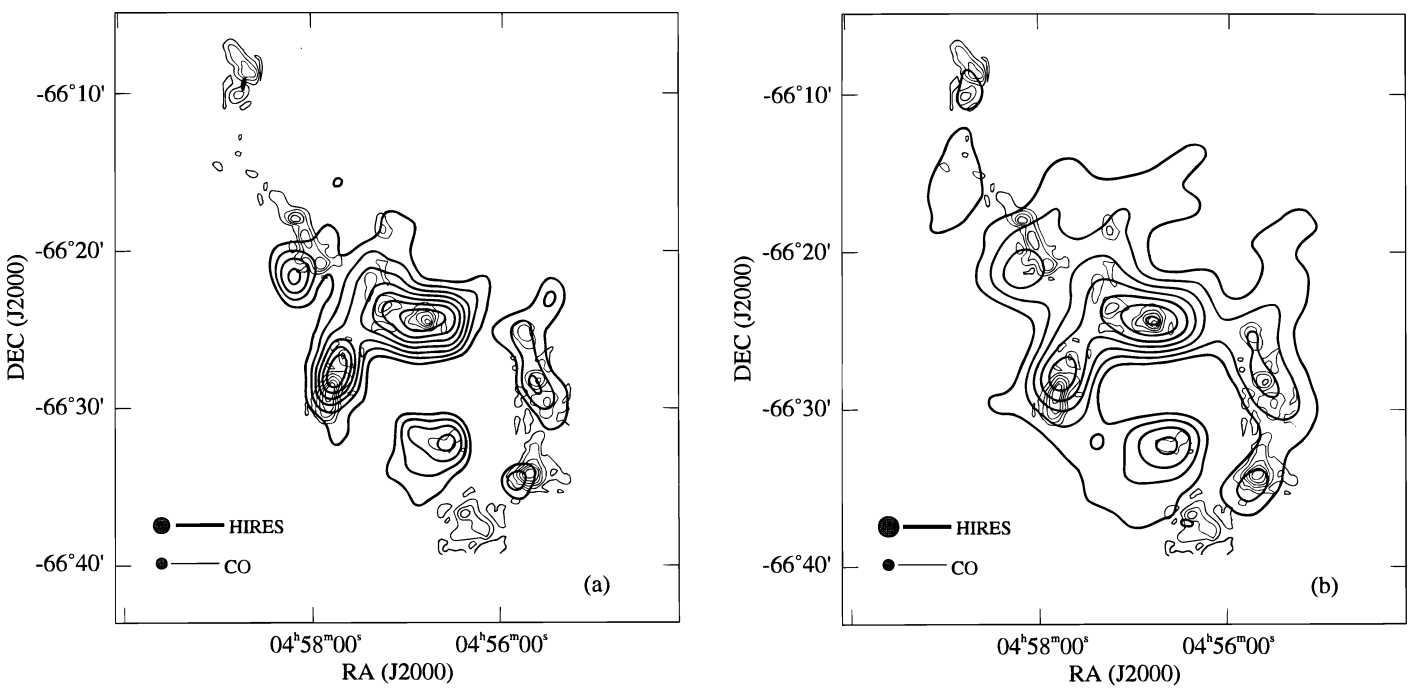

FIG. 3.—N11 *IRAS* HIRES emission maps shown with CO ($J = 1 \rightarrow 0$) integrated intensity (*light contours*) for comparison. (*a*) 60 μm map with log spaced contours at 35, 53, 79, 118, 178, 266, 400, 600 MJy sr^{-1}. (*b*) 100 μm map with log spaced contours at 50, 78, 121, 187, 290, 451, 700 MJy sr^{-1}. The CO ($J = 1 \rightarrow 0$) contours are 1, 3, 5, 7, 9, 11, 13, 15 K km s^{-1} in both figures. Note: the CO data do not extend over the full area of the map; therefore, some of the lowest contours are not closed.

TABLE 1

FIR Sources

Source (1)	SEST–Key Programme CO Peak[a] (2)	LI-LMC Number[b] (3)	R.A. (J2000) (4)	Decl. (J2000) (5)
30DOR-S.....	30DOR-SOUTH-01, 02, 03, 04, 05, 06, 07	1521	05 39 54	−71 09 47
30DOR-C03.....	30DOR-CENTER-03	1508	05 39 53	−70 08 18
30DOR-C04.....	30DOR-CENTER-04	1497	05 39 33	−70 13 52
30DOR-C07.....	30DOR-CENTER-07	...	05 40 43	−70 10 07
30DOR-C08.....	30DOR-CENTER-08, 09, 11	...	05 40 57	−70 20 18
30DOR-C12.....	30DOR-CENTER-12	1562	05 41 06	−70 23 39
30DOR-C13.....	30DOR-CENTER-13	1550	05 40 47	−70 28 22
30DOR-C16.....	30DOR-CENTER-16, 17A, 17B, 17C	...	05 40 58	−70 34 08
30DOR-C20.....	30DOR-CENTER-20	1536	05 40 24	−70 36 46
N11-01.....	N11-01A, 01B	248	04 57 45	−66 27 48
N11-02.....	N11-02A, 02B	205	04 56 20	−66 37 15
N11-03.....	N11-03A, 03B	192	04 55 50	−66 34 38
N11-04.....	N11-04A, 04B	190	04 55 34	−66 28 44
N11-05.....	N11-05	195	04 55 46	−66 25 23
N11-06A.....	N11-06A, 06C	217	04 56 52	−66 24 27
N11-06B.....	N11-06B	226	04 57 11	−66 23 19
N11-07A.....	N11-07A, 07B	251	04 58 12	−66 21 51
N11-07C.....	N11-07C, 07F, 07G, 07H	268	04 59 07	−66 16 55
N11-08.....	N11-08	...	04 57 20	−66 20 36
N11-09.....	N11-09A, 09B, 09C	266	04 58 45	−66 09 15
N11-13.....	N11-13A, 13B	214	04 56 31	−66 32 11

Note.—Units of right ascension are hours, minutes, and seconds, and units of declination are degrees, arcminutes, and arcseconds.

[a] Several of the FIR clouds contain multiple CO peaks. See Kutner et al. 1996a, 1996b and de Graauw et al. 1996 for CO peak positions.

[b] LI-LMC numbers from the Leiden *IRAS*-LMC catalog (Schwering 1989).

emission is above the background (or the number within the CO defined cloud in ambiguous cases) times the HIRES pixel size. The 60 μm cloud size is used to calculate both the 60 μm and 100 μm fluxes since the higher resolution closer matches the CO cloud boundaries. The 60 μm and 100 μm background intensities used for each cloud are given in columns (5) and (6).

Table 3 contains the derived FIR properties for the GMCs listed in Table 2. The source names are listed in column (1). The background-subtracted cloud intensities, S_{60}, and S_{100}, are multiplied by the *IRAS* 60 μm and 100 μm bandwidths as given in the *IRAS* Explanatory Supplement and the cloud area to obtain a flux. Columns (2) and (3) contain the fluxes, F_{60}, and F_{100}, for each source at 60 μm and 100 μm, respectively.

In order to obtain a dust temperature, the intensities are color corrected assuming the FIR emission to be blackbody radiation modified by the dust emissivity, according to the method given in the *IRAS* Explanatory Supplement. The dust temperature, T_D, is determined from the ratio of S_{100}

TABLE 2

Observed FIR Properties

Source (1)	Area (10^3 pc^2) (2)	I_ν (60 μm) (10^6 Jy sr^{-1}) (3)	I_ν (100 μm) (10^6 Jy sr^{-1}) (4)	*BG* (60 μm) (10^6 Jy sr^{-1}) (5)	*BG* (100 μm) (10^6 Jy sr^{-1}) (6)
30DOR-S.....	3.0	68	110	10	15
30DOR-C03.....	3.0	10	48	3	3
30DOR-C04.....	6	20	60	3	4
30DOR-C07.....	4.8	12	39	3	1
30DOR-C08.....	7.0	3.8	25	3	2
30DOR-C12.....	3.7	8.4	26	3	3
30DOR-C13.....	2.7	11	28	4	4
30DOR-C16.....	5.8	10	32	4	5
30DOR-C20.....	3.5	5.2	15	4	5
N11-01.....	6.7	92	150	4	11
N11-02.....	1.3	17	40	3	6
N11-03.....	4.6	26	57	3	7
N11-04.....	5.1[a]	38	79	4	9
N11-05.....	5.1[a]	38	81	4	11
N11-06A.....	6.4[a]	200	310	5	12
N11-06B.....	0.9[a]	80	160	5	14
N11-07A.....	4.9	47	100	5	15
N11-07C.....	5.1	17	53	6	17
N11-08.....	1.7	37	84	5	15
N11-09.....	3.0	14	37	7	20
N11-13.....	4.6	65	110	4	8

[a] Cloud boundaries determined from CO emission.

TABLE 3

DERIVED FIR PROPERTIES

SOURCE (1)	F_{60} (10^{-13} W m^{-2}) (2)	F_{100} (10^{-13} W m^{-2}) (3)	T_D (K) $\beta = 1.0$ (4)	$\beta = 1.5$ (5)	$\beta = 2.0$ (6)	L_{FIR} (10^4 $L_\odot$) (7)
30DOR-S	18	11	40	36	33	41
30DOR-C03	2.2	5.5	24	22	21	15
30DOR-C04	10	13	30	28	26	39
30DOR-C07	4.5	7.2	27	26	24	21
30DOR-C08	0.5	6.5	15	15	14	14
30DOR-C12	2.0	3.5	27	25	23	10
30DOR-C13	2.1	2.6	30	28	26	7.6
30DOR-C16	4.0	6.4	27	25	24	19
30DOR-C20	0.4	1.4	22	20	19	3.5
N11-01	61	38	40	36	33	140
N11-02	1.9	1.8	34	31	29	5.5
N11-03	11	9.2	35	32	29	29
N11-04	18	14	36	33	30	46
N11-05	18	14	36	33	30	46
N11-06A	130	76	42	37	34	280
N11-06B	7.1	5.4	37	33	31	18
N11-07A	21	17	36	33	30	54
N11-07C	6.0	7.4	30	28	26	21
N11-08	5.5	4.6	35	32	29	15
N11-09	2.2	2.0	34	31	29	6.3
N11-13	29	18	40	36	33	65

and S_{60}, using a dust emissivity index (β) according to

$$\frac{S_{100}}{S_{60}} = \left(\frac{\lambda_{60}}{\lambda_{100}}\right)^{\beta+3} \frac{\exp\left(hc/\lambda_{60}kT_D\right) - 1}{\exp\left(hc/\lambda_{100}kT_D\right) - 1}, \qquad (1)$$

by interpolating T_D for the measured flux ratio from a table of ratios for known temperatures. The color corrections for S_{60} and S_{100} are temperature dependent, so the corrected intensities are used to determine a new temperature, which then determines new color correction factors. This process is iterated until the temperature is unchanged within the limits of error. Columns (4), (5), and (6) give the dust temperature for each cloud for $\beta = 1$, 1.5, and 2.0, respectively. We used the correction given in Helou et al. (1988) to get the FIR flux between 42.5 μm and 122.5 μm for each cloud. The correction is valid for a thermal source with T between 20 and 80 K and emissivity index, β (dust emissivity $\propto \nu^\beta$) between 0 and 2. Using this value, the S_{100}/S_{60} color temperature, and assuming an emissivity of $\beta = 1$, a total FIR flux from 1 to 500 μm is determined according to the method in Cataloged Galaxies and Quasars (1985). From this FIR flux, and a distance to the LMC of 50.1 $\pm$ 3.1 kpc (Panagia et al. 1991), we calculate the total FIR luminosity, L_{FIR}, for the individual molecular clouds. The values of L_{FIR} are listed in column (7).

A comparison of the derived FIR and CO cloud properties is presented in Table 4. Column (1) gives the source names. For ease of comparison, column (2) repeats L_{FIR}.

TABLE 4

COMPARISON OF FIR AND CO PROPERTIES

Source (1)	L_{FIR} (10^4 $L_\odot$) (2)	L_{CO} (10^4 K km s^{-1} pc^2) (3)	M_{VIR} (10^5 $M_\odot$) (4)	L_{FIR}/M_{VIR} ($L_\odot/M_\odot$) (5)
30DOR-S	41	1.74	2.0	2.1
30DOR-C03	15	2.75	5.0	0.31
30DOR-C04	39	1.82	5.0	0.78
30DOR-C07	21	2.79	5.3	0.39
30DOR-C08	14	4.72	10	0.14
30DOR-C12	10	3.01	2.2	0.45
30DOR-C13	7.6	0.786	1.0	0.73
30DOR-C16	19	2.35	8.8	0.21
30DOR-C20	3.5	0.640	1.7	0.21
N11-01	140	1.10	4.8	2.8
N11-02	5.5	0.866	1.4	0.40
N11-03	29	0.332	7.3	0.40
N11-04	46	0.531	2.5	1.9
N11-05	46	0.340	0.92	5.0
N11-06A	280	0.551	4.0	7.0
N11-06B	18	0.296	1.2	1.5
N11-07A	54	0.805	2.9	1.9
N11-07C	21	0.689	2.7	0.80
N11-08	15	0.191	0.49	3.0
N11-09	6.3	0.748	1.1	0.56
N11-13	65	0.206	0.44	15

Column (3) is the CO luminosity, L_{CO}, of the cloud in the CO ($J = 1 \rightarrow 0$) line. This is determined from the average integrated intensity of the cloud multiplied by the cloud area. Column (4) contains the virial mass of the cloud, M_{VIR}, calculated using an expression appropriate for a uniform density cloud. Issues in using virial masses for these clouds are discussed more fully by Kutner et al. (1996b). Elmegreen (1989), by modeling virialized clouds, reproduced many of the results of three Milky Way CO studies using both ^{13}CO (Falgarone & Puget 1986; Pérault 1987) and ^{12}CO (Solomon et al. 1987). These results give us confidence in using virial mass as an estimator of cloud mass, especially for statistically significant ensembles. That is, M_{VIR} may not be a good indication of mass for any one cloud but is appropriate for the average of a group. Column (5) is the star formation activity, defined as the ratio of the FIR luminosity to virial mass, L_{FIR}/M_{VIR}. Star formation activity is essentially the star formation rate per unit cloud mass.

4. DISCUSSION

4.1. *Far-Infrared and CO Morphology*

From Figures 1, 2, and 3 we see that there is good correspondence between the FIR emission and the CO emission. In 30DOR-SOUTH, there is no significant FIR emission in the 1 deg^2 HIRES field outside of the region covered by the CO data. In 30DOR-CENTER, there is some FIR emission north of the region shown in Figure 1 toward 30 Doradus. In addition, there is one strong FIR peak (LI-LMC 1471) southwest of the area in Figure 1. In the N11 1 deg^2 field, there is some low-level emission northeast of the area shown in Figure 3. There is also one significant peak to the southwest (LI-LMC 144). In both cases, these emission peaks are clearly separated from the emission shown in Figures 1 and 3, respectively.

The CO-FIR morphology differs in the N11 and 30DOR-CENTER region. In 30DOR-CENTER, there is significant extended CO emission between the individual molecular peaks. The FIR emission follows the overall molecular emission throughout 30DOR-CENTER. Of the eight clouds for which the FIR and CO emission are well associated, six contain only a single CO peak within the FIR emission. A peak is defined as a local maximum in (α, δ, v_{lsr}) space. Two others consist of multiple CO peaks: 30DOR-C08 contains three distinct CO peaks, and 30DOR-C16 contains two peaks. These clouds could not be resolved in FIR, either because of the lower resolution of the HIRES images compared to the CO maps or because the FIR emission for these regions really does run together. In calculating the CO luminosity, virial mass, and star formation activity for these clouds, the CO data for each of the peaks were added. The results from these composite clouds will still be useful to us, as the star formation per unit mass will be the average over the GMCs contained within the measured "cloud"; thus, we can still make comparisons with GMCs in other regions. The clouds in the 30DOR-CENTER region vary in diameter from about 40 to 100 pc. In addition, in 30DOR-CENTER there are three regions in which molecular peaks have no significant associated FIR emission. One region lies to the north, containing the CO clouds 30DOR-CENTER-1 (J2000: R.A. = $5^h39^m52^s$, decl. = $-70°02'53''$) and 30DOR-CENTER-2 (R.A. = $5^h39^m21^s$, decl. = $-70°06'51''$). The other two regions lie to either side of the line of emission extending southward in Figure 1. They are 30DOR-CENTER-14 (R.A. = $5^h41^m03^s$, decl. = $-70°29'58''$) and 30DOR-CENTER-15 (R.A. = $5^h39^m48^s$, decl. = $-70°27'53''$). For all these peaks, the FIR emission at either 60 μm, 100 μm, or both was below the background value used for that location.

The CO emission in the N11 region shows more distinctive peaks than in the 30DOR-CENTER region. There is also very little molecular emission between the peak areas. This made for easier determination of the cloud boundaries in N11. The CO peaks in N11 are for the most part in closely spaced, $\sim 1'$–$2'$, groups with little or no CO emission between the groups. This means that of the 12 clouds observed in N11, nine consist of more than one individual molecular peak. The clouds N11-05, N11-06B, and N11-08 all contain only one CO peak. The clouds N11-01, 02, 03, 04, 06A, 07A, and 13 all contain two molecular peaks. N11-09 and N11-07C contain 4 and 6 CO peaks respectively. The N11 clouds are for the most part less CO luminous than those in 30DOR-CENTER and 30DOR-SOUTH.

These results are comparable to those found in the outer Galaxy by Mead et al. (1987), in which infrared sources were found to be closely associated with molecular peaks. They also found some CO peaks with no corresponding infrared emission. The presence of GMCs with no star formation is not unexpected. Even in the inner Galaxy, where CO emission is stronger on average than in the LMC or outer Galaxy (see, e.g., Cohen et al. 1988 and Israel et al. 1993 for the LMC and Mead & Kutner 1988 for the outer Galaxy), there are many molecular clouds with little or no star formation activity. For example, Chiar et al. (1994) found that a large fraction, $\sim 60\%$, of the gas at the tangent point of the Scutum arm was cool ($T < 10$ K) with no evidence for star formation.

It is interesting to compare our data with other tracers of star formation. N11 is ideally suited for this comparison. Because of its abundant Hα emission and unobscured O and B stars, extensive work has been done on this region using other star formation tracers (see, e.g., Walborn & Parker 1992; Meaburn et al. 1989; Heydari-Malayeri, Niemla, & Testor 1987). Figure 4 is an Hα image from Walborn & Parker (1992) on which 60 μm contours have been overlaid. The first thing evident from this figure is the almost exact match of the FIR and Hα emission. The FIR emission peaks all correspond to Hα peaks, and the extended FIR emission overlays the extended Hα emission, both of which trace the same shell-like structures. This good match is not surprising. It merely tells us that there is dust in and/or around the ionized hydrogen gas and that the dust is being heated by the same sources that are ionizing the gas.

A comparison of Figure 4 with Figure 3*a* reveals that the CO and Hα emission also show strong spatial correlation. Both trace the ringlike structure of N11. The CO generally follows the Hα emission; however, the CO and Hα peaks are not always coincident. In one case, N11-07A in the northeast of N11, the CO and Hα peaks are clearly separated. Again, this is not surprising; the Hα emission comes from ionized hot gas where it is expected CO would not survive. Here we could be looking at an example of an H II region in which a bright O or B star or association has burned away the edge of the parent molecular cloud. By comparing the FIR and CO emission from such a region,

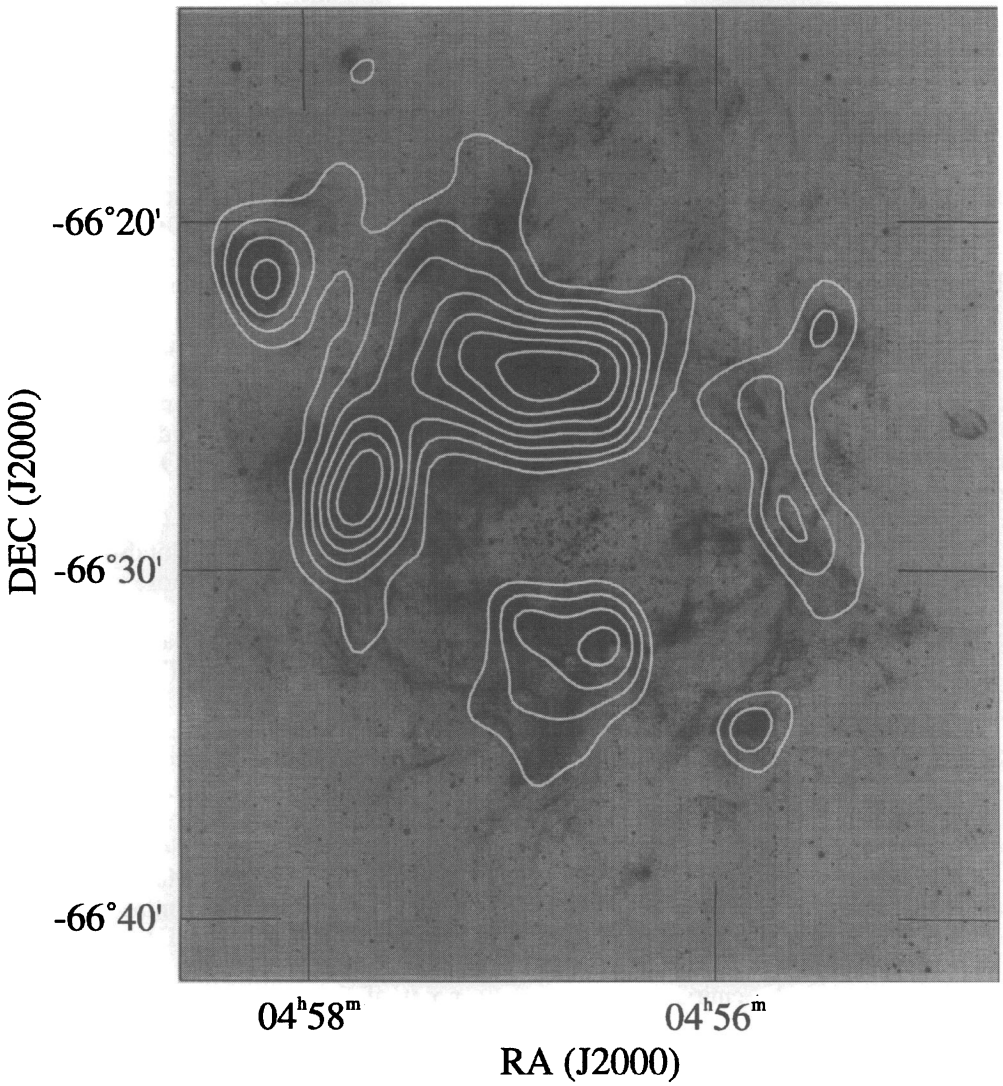

FIG. 4.—Hα + [N II] photograph of N11 courtesy of Nolan R. Walborn, shown with 60 μm *IRAS* HIRES contours. The 60 μm contours indicate the same values as in Fig. 3*a*. The excellent correspondence between the FIR and Hα emission demonstrates the suitability of FIR emission as a tracer of massive star formation.

we are still getting an indication of the clouds star formation activity as it is likely that the CO traces the GMC from which the stars in the H II region formed.

The good correspondence of the FIR emission with the Hα emission confirms that FIR can be used as a tracer of massive star formation. The lack of Hα emission (see, e.g., Davies, Elliott, & Meaburn 1976, Plates I, X) in 30DOR-CENTER and 30DOR-SOUTH likely results from much more obscuration by dust in this region compared to N11. Perhaps this is merely a younger region in which the star formation has not had time to burn away the parent GMCs. This is consistent with the estimate by Walborn & Parker (1992) that star formation in N11 is about 2×10^6 yr more advanced than that in 30 Dor.

4.2. *FIR Results*

In order to help verify our HIRES measurements, we have compared our results with the FIR survey of the LMC done by Schwering (1989). In this survey, Schwering used the *IRAS* Pointed Observations of the LMC to make maps of the entire LMC at all four *IRAS* bands. Sources with intensity greater than 3, 2, 1, and 0.5×10^{-7} W m^{-2} sr^{-1} at 12, 25, 60, and 100 μm, respectively, are listed in the LI-LMC catalog. Of our 21 detected sources, 17 correspond with LI-LMC cataloged sources, while the other four have no nearby matches. In 30DOR-CENTER, five of the eight sources have matches, and 11 of 12 sources in N11 have matches in the LI-LMC catalog. At 60 μm, the intensities of our sources match those of the LI-LMC sources reasonably well (all but two within 30%) and are for the most part higher than the LI-LMC values. At 100 μm, the intensities differ more from each other, with our intensities ranging from 10% to 80% higher than the LI-LMC values. These differences can be attributed to the different resolution used in the two measurements and the different background values subtracted. The resolution of the HIRES data is higher than the survey data by a factor of ~3. Schwering interpreted diffuse emission in the vicinity of a source as background. With the improved resolution of the HIRES data, this diffuse emission can be associated with individual sources. This can explain why our intensities, especially at 100 μm, are consistently higher than the LI-LMC values.

There are two main difficulties in calculating the L_{FIR} values given in Table 5. The first is that the 60 μm and

100 μm morphologies do not exactly correspond for some of the measured clouds. The better resolution of the 60 μm data allows us to distinguish some clouds at 60 μm and not at 100 μm. Since we use the molecular data to determine the cloud boundaries in these cases, this does not present a real difficulty. In addition, we measure the FIR intensities a few pixels beyond the CO boundaries to include FIR emission from the cloud edges. However, there are two cases where, at 100 μm, the dividing line between clouds cannot be distinguished. These are N11-04 and 05 and N11-06A and 06B. In these clouds, the 100 μm emission cannot, by itself, be associated with an individual cloud. The 100 μm fluxes from these clouds are therefore not certain. In the case of N11-04 and N11-05, where the two fluxes are approximately equal, the error in the flux associated with each cloud could be significant. The flux of N11-06A is more than 10 times that of N11-06B. As such, the percentage error due to confusion in the N11-06A flux is small, while that of N11-06B could be large. In 30DOR-CENTER, all of the measured clouds were distinguishable at both 60 μm and 100 μm.

The second difficulty in the calculation of $L_{\rm FIR}$ was the lack of long-wavelength data. As mentioned above, the 60 μm and 100 μm *IRAS* data give a FIR flux only between 42.5 μm and 122.5 μm and require a model estimate for emission out to 500 μm. We may therefore be missing emission from the coolest dust, any with an emission spectrum that peaks longward of 122.5 μm ($T_D \leq 20$ K), in the measure of $L_{\rm FIR}$. The dust temperatures given in Table 3 are consistent with the values used in our corrections for total FIR emission, however. In addition, the temperatures within each region are similar, giving us confidence that we are getting reasonable temperatures for the dust which *IRAS* is capable of detecting.

The mean value of $L_{\rm FIR}$ for all the LMC clouds is $\langle L_{\rm FIR}({\rm LMC})\rangle = 4.3 \times 10^5\ L_\odot$. On average the N11 clouds are more luminous than those in the region south of 30 Doradus. The mean value of $L_{\rm FIR}$ for the 30DOR-CENTER region is $\langle L_{\rm FIR}({\rm CENTER})\rangle = 1.6 \times 10^5\ L_\odot$, and that for the N11 region is $\langle L_{\rm FIR}({\rm N11})\rangle = 6.0 \times 10^5\ L_\odot$. There is considerable spread in the values of $L_{\rm FIR}$, however; in particular, one very luminous cloud in N11, 6A, significantly raises the average there. Not including this most luminous cloud lowers the average to $4.0 \times 10^5\ L_\odot$, still higher than that for the 30DOR-CENTER region.

In 30DOR-CENTER, the mean dust temperature is $T_D = 25.2 \pm 4.9$ K. In N11, the mean temperature is $T_D = 36.1 \pm 3.1$ K. Both of these values were calculated using $\beta = 1.0$. In Figure 5 we plot the log of the 60 μm flux versus the log of the 100 μm flux for each of the clouds observed. Both fluxes are color corrected for the temperature given in Table 3. Also plotted are lines of flux at constant temperature ranging from 10 to 60 K, calculated from a modified blackbody (eq. [1]) with $\beta = 1.0$. From this figure and Table 3, we see that temperatures of the clouds in the 30DOR-CENTER region vary more widely than those in N11. This is another indication of the differences between these two regions of the LMC.

4.3. *Star Formation*

Far-infrared dust emission gives a measure of star formation by relating $L_{\rm FIR}$ to the luminosity of the embedded sources in a GMC (see, e.g., Petrosian, Silk, & Field 1972; Marston & Dickens 1988; DeGioia-Eastwood 1992). As a first approximation, $L_{\rm FIR}$ can be equated to the total Lyman-continuum luminosity ($L_{\rm lyc}$) of the embedded newly formed stars (Marston & Dickens 1988). This assumes that all of the Lyman-continuum radiation emitted by the embedded stars is absorbed by the dust and reradiated in the far-infrared. In this model, there is no heating of the dust by UV radiation longward of the Lyman limit. The result-

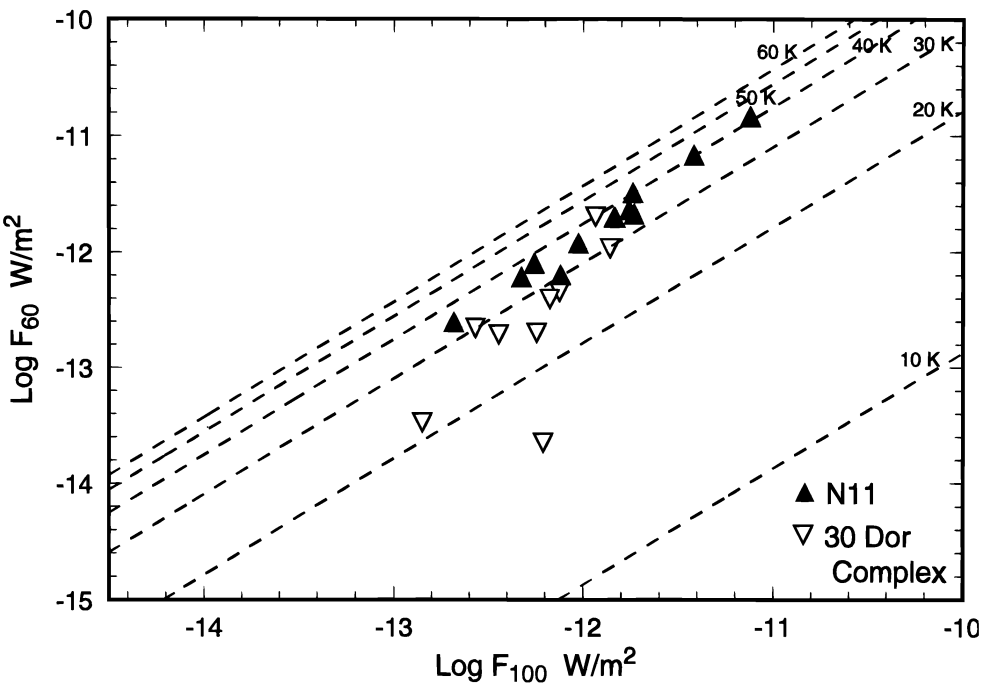

FIG. 5.—Log of far-infrared flux at 60 μm vs. 100 μm (F_{60} vs. F_{100}) for regions in 30DOR CENTER and SOUTH and N11. Shown with the data from the LMC clouds are lines of constant temperature calculated from a modified blackbody with dust emissivity, $\beta = 1.0$. The figure shows the GMCs from the region south of 30 Doradus (*open triangles*) separately from those in the N11 region (*filled triangles*) to emphasize the differences in the FIR emission from these two regions.

ant L_{lyc} can be used to estimate the number and type of embedded sources. This estimate is not unique in that, for example, five O8 stars have the same L_{lyc} as one O6 star. Because the dropoff of L_{lyc} with spectral type is so steep, though, this method will provide a reasonable estimate of the types of embedded stars. For example, it would require $\sim 2 \times 10^6$ B5 stars to provide the same L_{lyc} as one O6 star (Mezger, Smith, & Churchwell 1974). All derived spectral types are for ZAMS stars, as would be expected in young, star-forming clusters.

Using this method, the estimates of the minimum number of stars required to account for L_{FIR} observed from the LMC clouds range from $\sim$2.7 O4 stars in the case of N11-06A to $\sim$0.8 O8 stars for 30DOR-C20. The minimum numbers and types of stars associated with each cloud are listed in Table 5. These results for the N11 region are comparable with other estimates of stellar content. Walborn & Parker (1992) estimate that LH 10 (here N11-06A) contains several O3–O5 stars. Using vacuum ultraviolet (VUV) measurements of the flux of Lyman-continuum photons, Meaburn et al. (1989) estimate that 2.5 O5 stars are needed to excite LH 10. Israel (1980), based on radio observations, puts the value at seven O5 stars. From L_{FIR}, we obtain a value of 5.0 O5 stars, or 2.7 O4 stars, for the cloud N11-06A. Heydari-Malayeri & Testor (1985), based on Hβ emission, estimate the region of N11-06B is excited by a star with $T_{eff} \sim 44{,}000$ K. This corresponds to approximately an O7 star (Mezger et al. 1974) and is consistent with the estimate of 0.8 O6 or 1.9 O7 stars obtained from the far-infrared luminosity. For N11-01, we estimate one O4 star (two O5 stars) to account for L_{FIR}. The value from radio data is three O5 stars (Israel 1980) and 0.6 O5 star from VUV (Meaburn et al. 1989). Heydari-Malayeri et al. (1987) find one O3–O4 star and one O5 star in this region. We estimate 1.0 O5 stars in N11-07A based on L_{FIR}. Estimates from other sources are one, 0.05, and one O5 stars from radio (Israel 1980), VUV (Meaburn et al. 1989), and CCD imaging and spectroscopy (Heydari-Malayeri et al. 1987), respectively. Except for the VUV estimate in this last case, which Meaburn et al. (1989) states will have a large dependence on assumed extinction, all of the methods of ascertaining the numbers and types of embedded stars give comparable results. This gives us some confidence in using L_{FIR} to determine the amount of star formation in this manner.

A more detailed model of the far-infrared emission takes into account dust absorption of UV photons longward of the Lyman limit (see, e.g., DeGioia-Eastwood 1992). In this case, the far-infrared luminosity can be written as

$$L_{FIR} = L_{lyc} + (1 - e^{-\tau'})L_{UV} \, . \quad (2)$$

Here, L_{UV} is the stellar luminosity at $\lambda > 912$ Å, and τ' is the UV absorption optical depth of the dust. If τ' is known for a particular cloud, then L_{FIR} can be compared with L_{lyc} and L_{UV} for stars of different spectral types to determine the numbers and types of stars embedded within that GMC.

A value for τ' can be estimated from the 100 μm optical depth (τ_{100}) as follows. Using the extinction curve of Draine & Lee (1984) for a mixture of graphite and silicate grains (Mathis, Rumpl, & Nordsieck 1977), the column density of hydrogen (N_H) can be estimated as $N_H = 1.6 \times 10^{24}$ cm$^{-2}\tau_{100}$. Then, using this value for N_H, the optical depth at any wavelength can be read off the extinction curve. The absorption optical depth is related to the total optical depth (τ) by

$$\tau = \frac{\tau'}{1 - \omega} \quad (3)$$

(DeGioia-Eastwood 1992), where ω is the grain albedo given by Draine & Lee (1984) as a function of wavelength. The extinction optical depth at all wavelengths longer than 1215 Å is less than that at $\lambda = 1215$ Å. Thus, τ determined at the Lyα wavelength will result in an upper limit estimate for the contribution of L_{UV} to L_{FIR}. At $\lambda = 1215$ Å,

TABLE 5

STAR FORMATION TRACERS

Source (1)	L_{FIR} ($10^4 L_\odot$) (2)	L_{FIR}^{ISRF} ($10^4 L_\odot$) (3)	Number of Stars[a] (4)	Spectral Type (5)	τ_{100} (10^{-4}) (6)	τ'[b] (7)
30DOR-S.....	41	...	1.7	O6	4.5	0.73
30DOR-C03.....	15	...	1.6	O7	3.0	0.49
30DOR-C04.....	39	...	1.6	O6	3.2	0.52
30DOR-C07.....	21	...	0.9	O6	2.7	0.44
30DOR-C08.....	14	...	1.5	O7	4.3	0.70
30DOR-C12.....	10	...	1.1	O7	1.6	0.27
30DOR-C13.....	7.6	...	1.7	O8	1.5	0.25
30DOR-C16.....	19	...	0.8	O6	1.1	0.18
30DOR-C20.....	3.5	...	0.8	O8	0.46	0.08
N11-01.....	140	8.3	1.3	O4	2.2	0.36
N11-02.....	5.5	0.52	1.2	O8	0.65	0.10
N11-03.....	29	2.8	1.2	O6	1.0	0.16
N11-04.....	46	3.6	0.8	O5	1.2	0.19
N11-05.....	46	4.9	0.8	O5	1.6	0.27
N11-06A.....	280	10	2.7	O4	3.0	0.49
N11-06B.....	18	1.4	0.8	O6	2.9	0.47
N11-07A.....	54	5.9	1.0	O5	2.1	0.35
N11-07C.....	21	5.1	0.9	O6	1.7	0.28
N11-08.....	15	1.9	1.5	O7	1.9	0.31
N11-09.....	6.3	1.4	1.4	O8	0.76	0.12
N11-13.....	65	3.6	1.2	O5	1.3	0.21

[a] See text for discussion of stellar content.
[b] Absorption optical depth calculated at $\lambda = 1215$ Å.

$\tau = 1.7 \times 10^{-21}$ cm^2 N_H and $\omega = 0.4$ (Draine & Lee 1984). From this, τ' is calculated for each cloud. τ_{100} and τ' are listed in Table 5. As a check, we calculate the average τ' for the N11 clouds as 0.28 with a standard deviation of 0.13. DeGioia-Eastwood (1992) estimated $\tau' = 0.32 \pm 0.11$ for the N11 region by extrapolating from visual extinction measurements. The two estimates agree within the limits of error.

Using these values of τ', we calculate the numbers of stars needed to account for the observed L_{FIR}, taking into consideration dust heating by UV radiation (eq. [2]). In no case does the minimum number of stars change by a whole star from the estimate based on the simplest model ($L_{FIR} = L_{lyc}$). There are large differences in the numbers of later type stars estimated by the two models, but as we have no way of differentiating between many late-type stars or a few early-type stars, we report only the minimum numbers. For this purpose, the simple model produces adequate results.

One additional consideration in measuring the star formation of a given GMC is determining what percentage of L_{FIR} is due to heating by embedded sources and what is due to heating by the general interstellar radiation field (ISRF). We are able to make an estimate of the UV luminosity of the ISRF using the method given in Wall et al. (1996) and the results of Meaburn et al. (1989). They estimate from thermal radio continuum that between seven and 15 O5 stars are present in N11, and from Hα emission, 13 O5 stars. Using 13 as an estimate of the number of O5 stars, we calculate a UV luminosity of $13 \times L_{UV}(O5) = 3.93 \times 10^6$ $L_\odot$ (Mezger et al. 1974). Dividing by the area of N11, roughly circular with a diameter of 350 pc (Meaburn et al. 1989), gives the surface luminosity due to the ISRF. The contribution to the far-infrared luminosity due to the ISRF (L_{FIR}^{ISRF}) is then calculated for each cloud from

$$L_{FIR}^{ISRF} = 40.9\ L_\odot\ \mathrm{pc}^{-2}(1 - e^{-\tau'})A\ , \qquad (4)$$

where A is the cloud area in pc^2. For the N11 clouds, this ranges from 4% to 26% of L_{FIR}, with an average of 12%. Counting all of these stars in determining the UV luminosity of the ISRF for N11 will result in an overestimate as some of them are embedded in molecular clouds and will have some of their UV radiation absorbed. However, even with this overestimate of the ISRF, the minimum number of embedded stars needed to account for the observed L_{FIR} did not change from our simplest model by a whole star for any of the N11 clouds. Since the errors in this correction are undoubtedly greater than the 12% average change in L_{FIR}, we do not feel justified in including this effect without a better estimate of the ISRF.

4.4. *Comparison with Milky Way Clouds*

In order to compare the properties of LMC molecular clouds with those of Milky Way clouds, we need to use similar studies of the inner and outer Galaxy. For the inner Galaxy, we use the study of Scoville & Good (1989). The outer Galaxy work summarized in Mead et al. (1990) is very similar to this study and is therefore useful as a direct comparison. It is important to understand any biases in these surveys before comparing them. In our study, the CO maps were made for two regions that a large-scale CO ($J = 1 \rightarrow 0$) survey of the LMC showed contained significant emission. Details of the CO survey biases are available in Kutner et al. (1996a, 1996b) and de Graauw et al. (1996). We did not introduce any additional bias in the FIR portion of this study, in that we used all of the FIR data for which there was a CO correspondence. However, there is a bias toward clouds with stronger CO emission compared to other regions in the LMC. The two Milky Way surveys also show some bias toward the largest clouds. Mead et al. (1990) discusses in detail the biases in both the inner and outer Galaxy studies that we used.

Though all of these studies are biased toward the biggest, brightest clouds, there are some differences in biases that affect our comparison. Clouds in the outer Galaxy are more distinct than clouds in the molecular ring. In addition, Galactic geometry provides us with cleaner lines of sight in the outer Galaxy than in the molecular ring. Together, these mean that we can detect lower luminosity clouds in the outer Galaxy than in the molecular ring. Lines of sight in the LMC are relatively clean, as in the outer Galaxy. However, at the greater distance of the LMC, it is harder to detect lower luminosity objects. Therefore, it should not be surprising that the lowest FIR luminosity clouds are found in the outer Galaxy. This does not necessarily imply that outer Galaxy clouds are inherently less luminous. Clouds of this low luminosity would simply have been missed in the molecular ring and LMC studies.

We are working on a detailed analysis to compare the statistical properties of the star formation activity in these environments. However, it is useful to start by considering average quantities. A comparison of our L_{FIR} data with that from the Milky Way studies shows that the average L_{FIR} for the LMC is approximately four times that of the outer Galaxy, but only $\sim$5% of the inner Galaxy value. The three values are $\langle L_{FIR}(\mathrm{LMC})\rangle = 4.3 \times 10^5$ $L_\odot$, $\langle L_{FIR}(\mathrm{outerGal.})\rangle = 1.0 \times 10^5$ $L_\odot$ (Mead et al. 1990), and $\langle L_{FIR}(\mathrm{innerGal.})\rangle = 91 \times 10^5$ $L_\odot$ (Scoville & Good 1989). Looking at individual L_{FIR} values reveals that there are some LMC clouds as luminous as all but the most FIR-luminous inner Galaxy clouds. This indicates that despite the on average lower (as compared to the inner Galaxy) L_{CO} and M_{VIR}, the LMC GMCs still undergo significant massive star formation.

In order to determine if there are differences between the two galaxies in the types of clouds undergoing star formation, we compare the star formation activity calculated from the three surveys. Star formation activity is a measure of the star formation per unit mass. It indicates not whether larger clouds form more stars, but whether they form more stars per unit mass than smaller clouds. We present these results in Figure 6, plotting $\log L_{FIR}/M_{VIR}$ against $\log M_{VIR}$. Shown are results from this study, along with those from the outer Galaxy study of Mead et al. (1990) and the inner Galaxy study of Scoville & Good (1989). The inner Galaxy results are separated into H II region clouds and non–H II region clouds, based on 5 GHz radio continuum emission. Here we have recalculated the virial masses of the inner Galaxy clouds in the same manner used for the outer Galaxy study and this work.

To estimate how detection limits impact our star formation activity results, we consider L_{FIR} from a cloud whose intensity is the minimum value we measured (i.e., the background values) and whose size is the average area of the clouds studied. This corresponds to a minimum L_{FIR} $\sim 3.6 \times 10^4$ $L_\odot$, using the average background values for 30DOR-CENTER. We then calculate L_{FIR}/M_{VIR} for virial masses over the range of those seen in the LMC clouds. The minimum L_{FIR}/M_{VIR} ranges from 0.36 $L_\odot/M_\odot$ (log

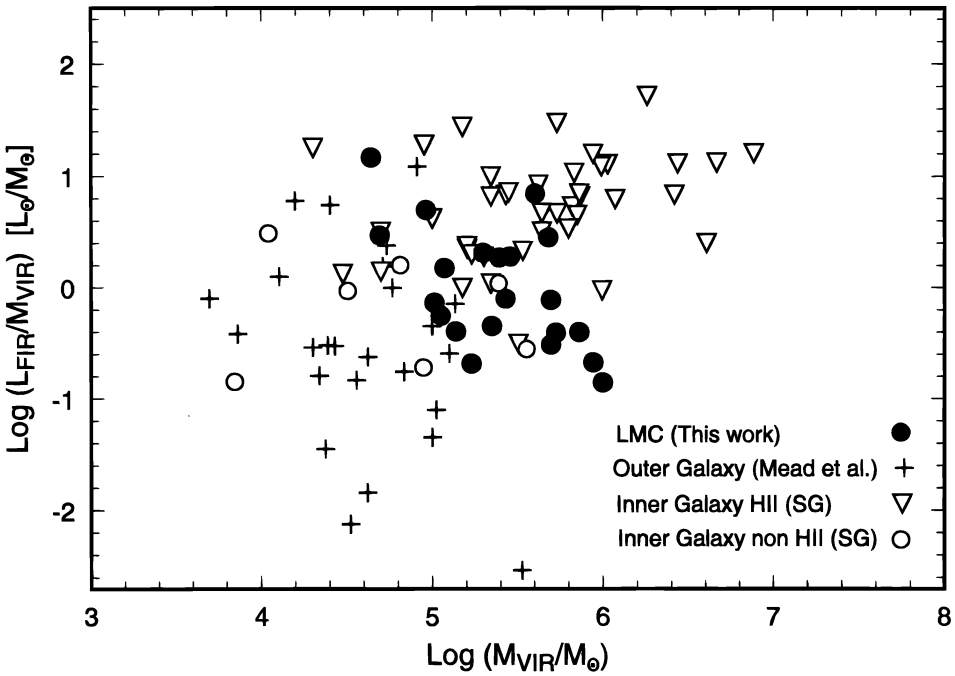

FIG. 6.—L_{FIR}/M_{VIR} vs. M_{VIR} for the LMC clouds (*filled circles*), shown along with data from the Milky Way studies discussed in the text. L_{FIR}/M_{VIR} is a measure of star formation activity, or the amount of star formation per unit mass that a GMC is undergoing. The LMC data show a wide range of star formation activity for any given mass, similar to what is seen in the Milky Way data. In addition, there is no correlation between star formation activity and cloud mass seen in the data from any of the regions represented.

$L_{FIR}/M_{VIR} = -0.45$) at $M_{VIR} = 10^5\ M_\odot$ to 0.036 $L_\odot/M_\odot$ ($\log L_{FIR}/M_{VIR} = -1.45$) at $M_{VIR} = 10^6\ M_\odot$. The minimum values calculated over the observed range of M_{VIR} lie just below the values for the observed LMC clouds in Figure 6. This indicates that the lower cutoff of L_{FIR}/M_{VIR} for the LMC clouds could be merely a detection limit. However, the estimated minimum L_{FIR} is within the range estimated for L_{FIR} due only to external heating in N11. Our detection limit is therefore near the value of L_{FIR} expected for clouds with no embedded sources in that region.

From Figure 6 we see that the LMC clouds have L_{FIR}/M_{VIR} values similar to the Milky Way clouds. The average value of L_{FIR}/M_{VIR} for the LMC clouds is 2.2 $L_\odot/M_\odot$. It is more meaningful to consider the two regions of the LMC separately. The mean L_{FIR}/M_{VIR} for the N11 region is 3.3 $L_\odot/M_\odot$, and that for the 30DOR-CENTER region is 0.4 $L_\odot/M_\odot$. The average value for the outer Galaxy clouds studied by Mead et al. (1990) is 1.6 $L_\odot/M_\odot$. The mean L_{FIR}/M_{VIR} for the inner Galaxy study is 8.0 $L_\odot/M_\odot$. If the H II and non–H II region clouds in this study are considered separately, the averages are 9.5 $L_\odot/M_\odot$ and 1.1 $L_\odot/M_\odot$, respectively (Scoville & Good 1989). Thus, on average the LMC clouds have star formation activities similar to GMCs in the outer Galaxy and the non–H II region clouds of the inner Galaxy.

The differences between the 30DOR and N11 regions can possibly be explained by looking at the appearances of the regions. The N11 clouds are widely separated, which suggests the aftermath of massive star formation (expanding H II regions, stellar winds, supernovae) has had a chance to drive away the material from all but the densest regions. In contrast, the 30DOR clouds are close together, which suggests that star formation is a more recent occurrence in that region. The destructive effects in the N11 region would mean that there is less molecular material left for a given amount of infrared luminosity. Again, this is supported by the suggestion that the N11 region is older than the 30 Doradus region by $\sim 2 \times 10^6$ yr (Walborn & Parker 1992).

In looking at Figure 6, we note a few important points:

1. For any cloud mass, there is at least a scatter of 2 orders of magnitude in the star formation activity. The large scatter can be in part explained by considering the N11 clouds. The estimates of heating due to the ISRF vary from 0.5 to $10 \times 10^4\ L_\odot$, corresponding to L_{lyc} from approximately two B0 to one O7 star (Mezger et al. 1974). Given the large uncertainty of the ISRF near any given cloud, this external heating is enough to account for the FIR emission from several of the GMCs in this study. The lower limit values of L_{FIR}/M_{VIR} may correspond to externally heated clouds, and the highest values to GMCs with several embedded early-O stars.This interpretation is supported by two trends that are seen in the figure. First, the outer Galaxy clouds probably have less external heating (Mead & Kutner 1988), so it is not surprising that they have some of the lowest FIR luminosities. Second, for the molecular ring, the non–H II region clouds form the lower bound of L_{FIR}. The scatter implies that for any given cloud mass, there is a range from virtually no star formation to strong massive star formation.

2. There is no obvious correlation of star formation activity with cloud mass.

3. There is no obvious difference in the trends for the three environments represented, particularly when one considers the biases in the various surveys, discussed above.

This scatter in L_{FIR}/M_{VIR} seems to argue against star formation scenarios in which clouds are built up from smaller parts until they reach some threshold mass at which point star formation begins. If this were the case, we would expect to see a cutoff in the formation of massive stars at some

value of M_{VIR}, below which massive star formation did not occur. We would also expect that the majority of clouds above that minimum mass should exhibit a high star formation activity. Neither of these effects is seen in Figure 6. This does not necessarily imply that GMCs are not built up out of smaller entities, only that a critical mass is not the sole requirement for the turn on of massive star formation.

5. SUMMARY

We have mapped FIR emission and compared it with CO ($J = 1 \rightarrow 0$) data from 21 GMCs in the LMC at comparable resolution. The FIR luminosities of these clouds range from 3.5×10^4 to 2.8×10^6 $L_\odot$. We used the SEST Key Programme CO data to calculate the virial masses of these clouds. The range of virial masses is 4×10^4 to 1×10^6 $M_\odot$. Comparing our results with those from similar work on Milky Way GMCs, we conclude the following:

1. Observed L_{FIR} indicates star formation consistent with 2.7 O4 stars for the brightest GMC to 0.8 O8 stars for the least FIR luminous. Stellar content estimates for GMCs in N11 are consistent with those from other methods. The estimate of the minimum numbers of stars required to account for L_{FIR} is relatively independent of UV absorption by dust and hence models of τ_{UV}.

2. The average L_{FIR} for the LMC clouds is comparable to that of the outer Galaxy clouds and significantly lower than the inner Galaxy value. The highest luminosity LMC clouds have L_{FIR} values as large as all but the most luminous inner Galaxy clouds.

3. Among the GMCs in the LMC, those from the two separate regions, the 30DOR-CENTER complex and N11, show significant differences in morphology and properties. The clouds in N11 are on average less CO luminous and have lower virial masses, $\langle M_{VIR}(\mathrm{N11})\rangle = 2.5 \times 10^5$ $M_\odot$ and $\langle M_{VIR}(\mathrm{CENTER})\rangle = 4.9 \times 10^5$ $M_\odot$. The N11 GMCs have, however, significantly higher average L_{FIR}, $\langle L_{FIR}(\mathrm{N11})\rangle = 6.0 \times 10^5$ $L_\odot$ and $\langle L_{FIR}(\mathrm{CENTER})\rangle = 1.6 \times 10^5$ $L_\odot$, thus resulting in a larger star formation activity for the N11 region clouds. In addition, the N11 clouds all have 60–100 μm flux ratios consistent with a small range of dust temperatures. The GMCs in 30DOR-CENTER show more variation in T_D.

4. The mean L_{FIR}/M_{VIR} for GMCs in the 30DOR-CENTER region of our study is 0.4 $L_\odot/M_\odot$, and for those in N11, 3.3 $L_\odot/M_\odot$. The mean for the Scoville & Good (1989) study of the inner Galaxy is 8.0 $L_\odot/M_\odot$. The mean for the outer Galaxy study (Mead et al. 1990) is 1.6 $L_\odot/M_\odot$.

5. It is significant that the star formation activity for the LMC shows a wide range of values for any given M_{VIR}, as is seen in both Milky Way studies.

6. The star formation activity of the LMC clouds, like that of both the inner and outer Galaxy clouds, shows no correlation with cloud mass. This seems discrepant with the idea that GMCs begin rapid star formation once they have reached some threshold size.

We would like to thank Don Mizuno for creating and repeatedly helping us with the *Reduce* CO data reduction and analysis package. Thanks to Jean Chiar and Colleen Stevens for providing reduced CO maps. We thank Deborah Levine and IPAC for their assistance with the HIRES data both during and after our visit. This work was supported by NASA grants NAG 2-677, NAG 5-1631, and NAG 5-2392.

REFERENCES

Aumann, H. H., Fowler, J. W., & Melnyk, M. 1990, AJ, 99, 1674
Bouchet, P., Lequeux, J., Maurice, E., Prevot, L., & Prevot-Burnichon, M.-L. 1985, A&A, 149, 330
Caldwell, D. A., & Kutner, M. L. 1993, in Proc. Heidelberg Conference: New Aspects of Magellanic Cloud Research, ed. B. Baschek, G. Klare, & J. Lequeux (Berlin: Springer), 171
———. 1997, in preparation
Cataloged Galaxies and Quasars Observed in the *IRAS* Survey. 1985, prepared by C. J. Lonsdale, G. Helou, J. C. Good, & W. Rice (Pasadena: Jet Propulsion Laboratory)
Chiar, J. E., Kutner, M. L., Verter, F., & Leous, J. 1994, ApJ, 431, 658
Cohen, R. S., Dame, T. M., Garay, G., Montani, J., Rubio, M., & Thaddeus, P. 1988, ApJ, 331, L95
Davies, R. D., Elliott, K. H., & Meaburn, J. 1976, MmRAS, 81, 89
DeGioia-Eastwood, K. 1992, ApJ, 397, 542
de Graauw, Th., et al. 1996, in preparation
Draine, B. T., & Lee, H. M. 1984, ApJ, 285, 89
Dufour, R. J. 1984, in IAU Symp. 108, Structure and Evolution of the Magellanic Clouds, ed. S. van den Bergh & K. S. de Boer (Dordrecht: Reidel), 353
Elmegreen, B. G. 1989, ApJ, 338,178
———. 1993, in Protostars and Planets III, ed. E. H. Levy & J. Lunine (Tucson: Univ. of Arizona Press), 97
Falgarone, E., & Puget, J. L. 1986, A&A, 162, 235
Fowler, J. W., & Melnyk, M. 1990a, Laundr Software Design Specification, IPAC 900808
———. 1990b, Yoric Software Design Specification, IPAC 900815
Helou, G., Khan, I. R., Malek, L., & Boehmer, L. 1988, ApJS, 68, 151
Heydari-Malayeri, M., Niemala, V. S., & Testor, G. 1987, A&A, 184, 300
Heydari-Malayeri, M., & Testor, G. 1985, A&A, 144, 98
IPAC User's Guide. 1993, ed. L. Fullmer, I. Khan, G. Laughlin, D. Levine, & R. Benson (JPL D-2416)
IRAS Catalogs and Atlases: Explanatory Supplement. 1985, ed. C. A. Beichmann, G. Neugebauer, H. J. Habing, P. E. Clegg, & T. J. Chester (JPL D-1855)
Israel, F. P. 1980, A&A , 90, 246
Israel, F. P., de Graauw, Th., van de Stadt, H., & de Vries, C. P. 1986, ApJ, 303, 186
Israel, F. P., et al. 1993, A&A, 276, 25
Koornneef, J. 1984, in IAU Symp. 108, Structure and Evolution of the Magellanic Clouds, ed. S. van den Bergh & K. S. de Boer (Dordrecht: Reidel), 333
Kutner, M. L., et al. 1996a, in preparation
Kutner, M. L., et al. 1996b, in preparation
Marston, A. P., & Dickens, R. J. 1988, A&A, 193, 27
Mathis, J. S., Rumpl, W., & Nordsieck, K. H. 1977, ApJ, 217, 425
Meaburn, J., Solomos, N., Laspias, V., & Goudis, C. 1989, A&A, 225 497
Mead, K. N. 1988, ApJS, 67, 149
Mead, K. N., & Kutner, M. L. 1988, ApJ, 330, 339
Mead, K. N., Kutner, M. L., & Evans, N. J., II. 1990, ApJ, 354, 492
Mead, K. N., Kutner, M. L., Evans, N. J., II, Harvey, P. M., & Wilking, B. A. 1987, ApJ, 312, 321
Mezger, P. G., Smith, L. F., & Churchwell, E. 1974, A&A, 32, 269
Panagia, N., Gilmozzi, R., Macchetto, F., Adorf, H. M., & Kirshner, R. P. 1991, ApJ, 380, L23
Pérault, M. 1987, Ph.D. thesis, Univ. of Paris
Petrosian, V., Silk, J., & Field, G. B. 1972, ApJ, 177, L69
Scalo, J. M. 1985, in Protostars and Planets II, ed. D. C. Black & M. S. Matthews (Tucson: Univ. of Arizona Press), 201
Scoville, N. Z., & Good, J. C. 1989, ApJ, 339, 149
Schwering, P. B. W. 1989, A&AS, 79, 105
Solomon, P. M., Rivolo, A. R., Barrett, J., & Yahil, A. 1987, ApJ, 319, 730
Walborn, N. R., & Parker, J. W. 1992, ApJ, 399, L87
Wall, W. F., et al. 1996, ApJ, 456, 556
Wouterloot, J. G. A., Henkel, C., & Walmsley, C. M. 1989, A&A, 215, 131